# Nuclear structure studies of $^{24}$F

L. Cáceres,[1] A. Lepailleur,[1] O. Sorlin,[1] M. Stanoiu,[1,2,3] D. Sohler,[4] Zs. Dombrádi,[4] S. K. Bogner,[5] B. A. Brown,[5] H. Hergert,[5] J. D. Holt,[5,6,7,8] A. Schwenk,[7,8] F. Azaiez,[2] B. Bastin,[1] C. Borcea,[3] R. Borcea,[3] C. Bourgeois,[2] Z. Elekes,[5] Zs. Fülöp,[4] S. Grévy,[1,9] L. Gaudefroy,[10] G. F. Grinyer,[1] D. Guillemaud-Mueller,[2] F. Ibrahim,[2] A. Kerek,[11] A. Krasznahorkay,[4] M. Lewitowicz,[1] S. M. Lukyanov,[12] J. Mrázek,[13] F. Negoita,[3] F. de Oliveira,[1] Yu.-E. Penionzhkevich,[12] Zs. Podolyák,[14] M. G. Porquet,[15] F. Rotaru,[3] P. Roussel-Chomaz,[1] M. G. Saint-Laurent,[1] H. Savajols,[1] G. Sletten,[16] J. C. Thomas,[1] J. Timàr,[4] C. Timis,[3] and Zs. Vajta[4]

[1]*Grand Accélérateur National d'Ions Lourds (GANIL), CEA/DSM-CNRS/IN2P3, Caen, France*
[2]*Institut de Physique Nucléaire, IN2P3-CNRS, F-91406 Orsay Cedex, France*
[3]*Institute of Physics and Nuclear Engineering IFIN-HH, P.O. Box MG-6, 077125 Bucharest-Magurele, Romania*
[4]*Institute for Nuclear Research (MTA Atomki), P.O. Box 51, H-4001 Debrecen, Pf.51, Hungary*
[5]*National Superconducting Cyclotron Laboratory and Department of Physics and Astronomy, Michigan State University, East Lansing, Michigan 48824, USA*
[6]*TRIUMF, 4004 Wesbrook Mall, Vancouver, British Columbia, V6T 2A3 Canada*
[7]*Institut für Kernphysik, Technische Universität Darmstadt, 64289 Darmstadt, Germany*
[8]*ExtreMe Matter Institute EMMI, GSI Helmholtzzentrum für Schwerionenforschung GmbH, 64291 Darmstadt, Germany*
[9]*Université Bordeaux 1, CNRS/IN2P3, Centre d'Études Nucléaires de Bordeaux Gradignan, UMR 5797, Chemin du Solarium, BP. 120, 33175 Gradignan, France*
[10]*CEA, DAM, DIF, F-91297 Arpajon, France*
[11]*Royal Institute of Technology, Stockholm, Sweden*
[12]*FLNR, JINR, RU-141980 Dubna, Moscow region, Russia*
[13]*Nuclear Physics Institute, AS CR, CZ-25068 Rex, Czech Republic*
[14]*University of Surrey, GU2 7XH Guildford, United Kingdom*
[15]*CSNSM, CNRS/IN2P3 and Université Paris-Sud, Bât 104-108, F-91405 Orsay, France*
[16]*Niels Bohr Institute, University of Copenhagen, Denmark*

The structure of the $^{24}$F nucleus has been studied at GANIL using the $\beta$ decay of $^{24}$O and the in-beam $\gamma$-ray spectroscopy from the fragmentation of $^{27,28}$Na, $^{25,26}$Ne, and $^{29,30}$Mg nuclei. Combining these complementary experimental techniques, the level scheme of $^{24}$F has been constructed up to 3.6 MeV by means of particle-$\gamma$ and particle-$\gamma\gamma$ coincidence relations. Experimental results are compared to shell-model calculations using the standard USDA and USDB interactions as well as *ab initio* valence-space Hamiltonians calculated from the in-medium similarity renormalization group based on chiral two- and three-nucleon forces. Both methods reproduce the measured level spacings well, and this close agreement allows unidentified spins and parities to be consistently assigned.

PACS number(s): 21.60.Cs, 23.20.Lv, 23.40.Hc, 27.30.+t

## I. INTRODUCTION

Nuclear forces play a decisive role in determining the structure of atomic nuclei, driving the creation and evolution of shell gaps, the onset of deformation, and development of halo structures, and in determining the limits of particle stability. The nuclear shell model provides a framework to determine the properties of nuclei from a set of single-particle energies (SPEs) and two-body matrix elements (TBMEs) defined in a given valence space outside some assumed inert core. When based only on two-nucleon (*NN*) forces within the valence space, the SPEs and TBMEs need suitable renormalization to experimental data to provide a precise description of nuclear structure. These "effective" SPEs and TBMEs implicitly capture the effects of many-body processes, such as core polarization, as well as neglected three-nucleon (3*N*) forces [1–4] and coupling to the particle continuum.

As the standard shell-model approach typically uses TBMEs that are independent of mass number *A* or simply scaled, it may become insufficient near the limits of stability, where the last nucleons are only loosely bound and have radial wave functions which extend to larger radii and couple to unbound states [5]. Reductions of the neutron-neutron TBME by 25% were required to model the structure of the neutron-rich C isotopes, which are a factor of 2 less bound than the O isotopes [6,7]. More recently, the study of the weakly bound $^{26}$F nucleus, which can be viewed as an $^{24}$O core plus a deeply bound $d_{5/2}$ proton and an unbound $d_{3/2}$ neutron, has shown that a reduction of the $\pi d_{5/2}$-$\nu d_{3/2}$ TBME by about 20% better reproduced the energies of its $J = 1^+$, $2^+$, $4^+$ states [8]. In addition, recent theoretical calculations for states close to the neutron-separation threshold show that an increased role of coupling to the particle continuum may in part account for the modification of shell structures of dripline nuclei [9,10].

The fluorine isotopic chain is well suited to studying the evolution of valence-space interactions with increased valence neutron-to-proton asymmetry toward the dripline. Moreover, many F isotopes are located near the doubly magic $^{16}$O, $^{22}$O,

and $^{24}$O systems. Considering these O isotopes as almost inert cores, fluorine wave functions should then be weakly mixed, making possible the search for subtle effects related to their weak binding and proximity to the continuum. Located close to $^{22}$O and $^{24}$O, $^{24}$F is an excellent candidate for such a study, because its spectroscopy is expected to be relatively simple. As in $^{26}$F, states located near the neutron separation energy, $S_n = 3.840(10)$ MeV, could be influenced by effects arising from asymmetric proton-to-neutron binding.

In a simple shell-model picture, the lowest-lying states in $^{24}$F with spin-parity $2^+$ and $3^+$ can be considered pure $\pi d_{5/2} \otimes \nu s_{1/2}$ configurations on top of an $^{22}$O core, while $0^+$ and $1^+$ states are expected from $\pi s_{1/2} \otimes \nu s_{1/2}$ configurations. Close to the dripline, the excitation of one neutron to the $d_{3/2}$ orbits gives rise to the $I^\pi = 1^+$–$4^+$ multiplet due to the $\pi d_{5/2} \otimes \nu d_{3/2}$ coupling observed at low energy in $^{26}$F [8]. Configurations originating from neutron core excitations are also found below the neutron-separation threshold.

While previous $\beta$-decay studies [11,12] agreed on the $^{24}$O half-life (about 65 ms), deduced delayed-neutron emission probabilities differed significantly: $P_n = 58(12)\%$ in Ref. [11] and $P_n = 18(6)\%$ in Ref. [12]. From the latter work, it was expected that $82(6)\%$ of the $\beta$ strength would decay to bound states in $^{24}$F [12]. Because only 60% of the $\beta$-decay strength was observed, it was proposed that this missing strength may feed higher-lying $1^+$ excited state(s), likely of $\pi d_{5/2} \otimes \nu d_{3/2}$ origin, that could not be observed experimentally due to the lack of statistics. Three $\gamma$ transitions associated with the decay of $^{24}$O were observed [12], but the statistics were not sufficient to unambiguously establish a $^{24}$F level scheme. No other spectroscopic information was known on $^{24}$F before the present study.

To search for members of the $d_{5/2}$-$d_{3/2}$ multiplet, the spectroscopy of $^{24}$F has been studied using two complementary experimental methods in this work. First, $1^+$ states were accessed from the $\beta$ decay of $^{24}$O, which has an $I^\pi = 0^+$ ground state. In a separate experiment, higher-spin states were produced in the fragmentation of projectile nuclei leading to $^{24}$F. The results were then compared to shell-model calculations based on the benchmark USDA and USDB empirical Hamiltonians [13] as well as *ab initio* valence-space Hamiltonians derived from $NN + 3N$ forces [14]. The excellent agreement between these two calculations results in a robust description of the newly measured states.

## II. $\beta$ DECAY OF $^{24}$O

### A. Experimental setup

The $^{24}$O nucleus was produced via fragmentation of a $^{36}$S$^{16+}$ primary beam delivered by the GANIL facility in a 237 mg/cm$^2$ Be target placed at the entrance of the LISE spectrometer [15]. The energy and the average intensity of the primary beam were 77.6 MeV/u and 2 $e\,\mu$A, respectively. The projectile-like fragments were separated by the LISE achromatic spectrometer. A $^9$Be wedge-shaped degrader of 1066 mg/cm$^2$ was placed at the dispersive focal plane of LISE to improve the ion selection. As shown in Fig. 1 the selected nuclei were identified at the end of the spectrometer by means
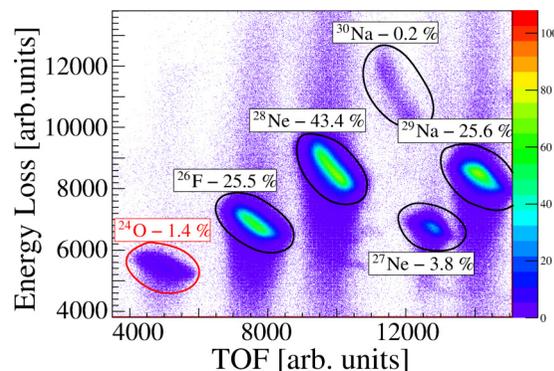


FIG. 1. (Color online) Energy loss versus time-of-flight identification matrix. The relative yields of the implanted ions are shown by different shades.

of their energy loss ($\Delta E$) in two silicon detectors of 500 $\mu$m thickness and their time-of-flight (TOF) referenced to the cyclotron radio frequency. An Al foil of adjustable inclination was placed after the two Si detectors to allow the implantation depth of the $^{24}$O ions into a 1 mm double-sided-silicon-strip detector (DSSSD) of $5 \times 5$ cm$^2$ with $16 \times 16$ strips. The pixels in the DSSSD were used to establish spatial and time correlations between the $\beta$ particles and the $^{24}$O parent. Energy thresholds of the individual strips were set to $\sim$80 keV. A 5-mm-thick Si(Li) detector was placed after the DSSSD to control the implantation depth of $^{24}$O.

Four segmented Ge clover detectors of the EXOGAM array [16] were placed around the DSSSD detector to provide $\beta$-$\gamma$ coincidences. A $\gamma$-ray efficiency $\varepsilon_\gamma$ of 6.5% at 1 MeV was extracted from the $\beta$ decay of $^{28}$Ne which was transmitted in the same setup and for which the intensities of the $\gamma$ transitions were known [17]. For each implanted nucleus, a $\beta$ efficiency ($\varepsilon_\beta$) of 63(3)% was extracted from the intensity ratio between an identified $\gamma$ line gated or ungated on the $\beta$-correlation condition. The relative $\gamma$-ray intensities were obtained from the $\varepsilon_\beta$ and $\varepsilon_\gamma$ values.

### B. Results

The $\beta$-gated $\gamma$-ray spectrum following the implantation of a precursor $^{24}$O nucleus between 0 and 250 ms is shown in Fig. 2(a). This time condition favors the observation of $\gamma$ rays associated with the decay of $^{24}$F while it suppresses all transitions belonging to contaminant nuclei or daughter activity. The previously reported $\gamma$ lines [12] at 521, 1309, and 1830 keV are clearly visible. All other observed transitions are not attributed to the decay of $^{24}$O.

A total of $\sim$10$^5$ $^{24}$O nuclei were implanted in the DSSSD detector, which is a factor of 10 larger than in Ref. [12]. The improved statistics obtained in the present work permitted a study of $\gamma\gamma$ coincidences [Fig. 2(b)], from which it was deduced that the $1^+$ level at 1830 keV is fed with $I_\beta = 57(4)\%$ and decays by a cascade of 521 and 1309 keV $\gamma$ rays. The ordering of these two transitions could not be determined unambiguously from the $\beta$-decay study because they have the same relative intensity (Table I). The in-beam experiment presented in Sec. III B shows that the 1309 keV $\gamma$ ray
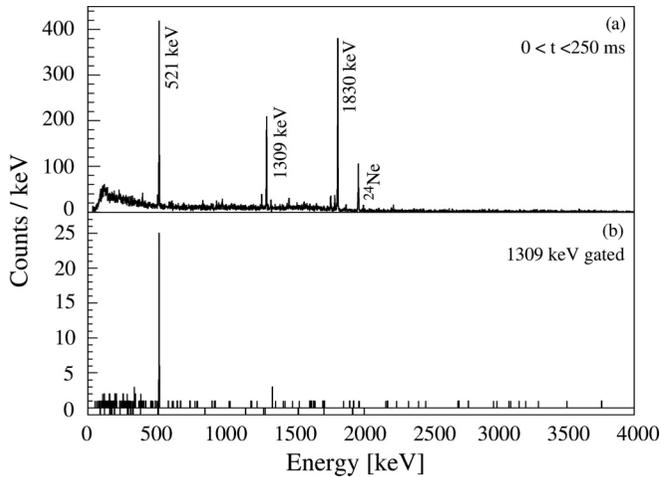
FIG. 2. (a) $\beta$-gated $\gamma$-ray spectrum following the implantation of $^{24}$O nuclei obtained in the 0–250 ms range. (b) $\gamma\gamma$-coincidence spectrum gated by the 1309 keV $\gamma$ ray.
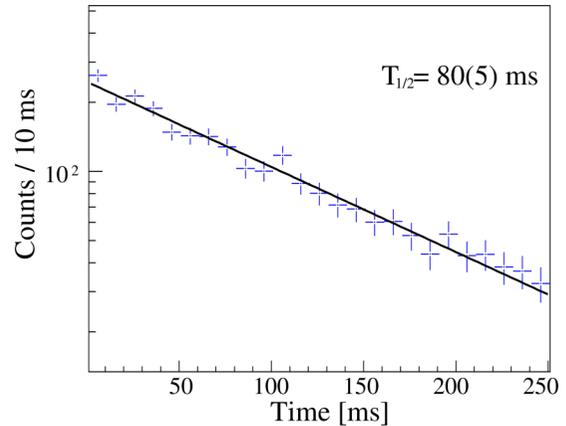


FIG. 3. (Color online) Background-subtracted summed time distribution gated on the 521, 1309, and 1830 keV $\gamma$ rays following the implantation of $^{24}$O nuclei. The fit with a single exponential decay curve yields $T_{1/2} = 80(5)$ ms.

feeds a level at 521 keV. The 1830 keV level decays by a competing branch directly to the ground state as well. The $\gamma$-ray energies, relative intensities, and branching ratios of the observed transitions are listed in Table I.

The background-subtracted summed time distribution of the 521, 1309, and 1830 keV $\gamma$ rays with respect to the $^{24}$O implantation is shown in Fig. 3. A fit with a single exponential decay curve yields a half-life of $T_{1/2} = 80(5)$ ms, in agreement with the $61^{+32}_{-19}$ ms value of Ref. [11] within the statistical uncertainties, but longer than the value of 65(5) ms reported in Ref. [12]. Using the $\beta$-decay $Q$ value and the absolute feeding intensity of the 1830 keV state, a $\log ft$ value of 4.25(6) has been obtained, which is consistent with an allowed Gamow-Teller transition.

The observational limit for the population of other $1^+$ states has been measured to be 1.0(4)%. The $\beta$-delayed neutron emission probability has been extracted to be $P_n = 43(4)\%$ from the yields of the 1830 and 1309 keV transitions normalized to the total number of $^{24}$O detected. This value is in agreement with $P_n = 58(12)\%$ previously reported in Ref. [11] but larger than the value of 18(6)% measured in Ref. [12].

In a separate setting of the LISE spectrometer, the $\beta$ decay of $^{24}$F was studied as well. From this data set the direct feeding to the $2^+$ state at 1981 keV and the $4^+$ state at 3963 keV in $^{24}$Ne were observed [18]. It establishes that the spin and parity

of the ground state of $^{24}$F is $3^+$. It follows that the 521 keV state is located between the $3^+$ ground state and the $1^+$ excited state at 1830 keV. As the 521 keV state is not populated directly in the $^{24}$O $\beta$ decay its spin and parity must therefore be $2^+$.

## III. IN-BEAM SPECTROSCOPY OF THE $^{24}$F NUCLEUS

### A. Experimental setup

The $^{24}$F nucleus was produced in a two-step reaction. A $^{36}$S$^{16+}$ primary beam of 77.5$A$ MeV with an average intensity of 6.5 $e\,\mu$A underwent fragmentation in a 398 mg/cm$^2$ C target placed between the two superconducting solenoids of the SISSI [19] device. The reaction products were separated and selected trough the ALPHA spectrometer by means of the B$\rho$-$\Delta E$-B$\rho$ method [15,20]. The transmitted cocktail beam was composed of $^{25,26}$Ne, $^{27,28}$Na, and $^{29,30}$Mg nuclei with energies ranging between 54 and 65 MeV/u. The identification of the beam ions was performed by the combined measurement of their time-of-flight (TOF) over a flight path of 80 m using two micro-channel plates and their energy loss in a plastic scintillator of 103.5 mg/cm$^2$ thickness located at the entrance of the SPEG spectrometer [21]. Two C foils of 51 mg/cm$^2$ thickness were placed before and after the plastic scintillator constituting a secondary "active" target. The $^{24}$F nuclei were produced in this secondary target through the fragmentation of $^{27}$Na. Once produced, the $^{24}$F nuclei were separated from other reaction residues in the SPEG spectrometer. The identification of the ions was performed on an event-by-event basis at the final focal plane of the SPEG by measuring their TOF with a plastic scintillator, and their energy loss ($\Delta E$) and position in an ionization and two drift chambers, respectively. In addition, 74 BaF$_2$ detectors of the Château de Cristal array surrounded the secondary target at an average distance of 30 cm. Prompt $\gamma$-ray emission was measured in coincidence with the nuclei identified at the final focal plane of SPEG. The photopeak efficiency of the array was 24%, 42%, and 29% for $\gamma$-ray energies of 100, 600, and 1300 keV, respectively.

TABLE I. Experimental energies, spin and parity assignments, transition energies, relative intensities per 100 decays, and $\gamma$ branching ratio (BR) for the excited states of $^{24}$F observed in the $\beta$ decay of $^{24}$O experiment.

| $E_i$ (keV) | $I_i^\pi \rightarrow I_f^\pi$ | $E_\gamma$ (keV) | $I_\gamma$ (/100 decays) | BR(%) |
|---|---|---|---|---|
| 521(1) | $2_1^+ \rightarrow 3_1^+$ | 521(1) | 21(2) | |
| 1830(1) | $1_1^+ \rightarrow 3_1^+$ | 1830(1) | 39(3) | 68(5) |
| | $1_1^+ \rightarrow 2_1^+$ | 1309(1) | 18(2) | 32(3) |

TABLE II. Experimental energies, tentative spin and parity assignments, transition energies, relative feeding intensities, and $\gamma$ branching ratios (BR) for the excited states in $^{24}$F obtained in the in-beam spectroscopy experiment.

| $E_i$ (keV) | $I_i^\pi \rightarrow I_f^\pi$ | $E_\gamma$ (keV) | $I_\gamma(\%)$ | BR(%) |
|---|---|---|---|---|
| 527(10) | $2_1^+ \rightarrow 3_1^+$ | 527(10) | 71(3) | |
| 1829(26) | $1_1^+ \rightarrow 3_1^+$ | 1827(11) | 17(2) | 77(10) |
| | $1_1^+ \rightarrow 2_1^+$ | 1309(22) | 5(1) | 23(5) |
| 2384(64) | $(4_1^+, 3_2^+) \rightarrow 3_1^+$ | 2384(64) | 7(3) | |
| 2739(14) | $(3_2^+, 4_1^+) \rightarrow 3_1^+$ | 2739(14) | 100(5) | |
| 3562(22) | $(2_3^+, 4_2^+) \rightarrow 3_1^+$ | 3562(22) | 47(5) | |
| 3639(42) | $(1_2^+, 2_2^+) \rightarrow 2_1^+$ | 3118(33) | 34(3) | |

## B. Results

Prompt $\gamma$ rays observed in coincidence with the $^{24}$F nuclei identified in SPEG are listed in Table II. The singles $\gamma$-ray spectrum of $^{24}$F is shown in Fig. 4. The three $\gamma$ rays at 527(10), 1309(22), and 1827(11) keV correspond, within the experimental uncertainties, to those observed in the $\beta$ decay of $^{24}$O at 521(1), 1309(1), and 1830(1) keV, respectively. The excitation energy of the 1829(26) keV state has been extracted by the weighted average of the energies of the two decay branches. It is in agreement with the value obtained in the $\beta$-decay data set. The $\gamma\gamma$ coincidence between the 527 and 1309 keV transitions [Fig. 5(a)] is confirmed. The ordering of the two transitions is obtained from their relative intensity; since the 527 keV $\gamma$-ray intensity is much larger than that of the 1309 keV transition (Table II), the 527 keV state is placed below. It can be fed directly in the reaction and/or by other higher-lying excited states. In addition, four new transitions have been observed between 2200 and 4000 keV. To get a reasonable line shape, the response function of the BaF$_2$ array was simulated using the GEANT4 package. In the
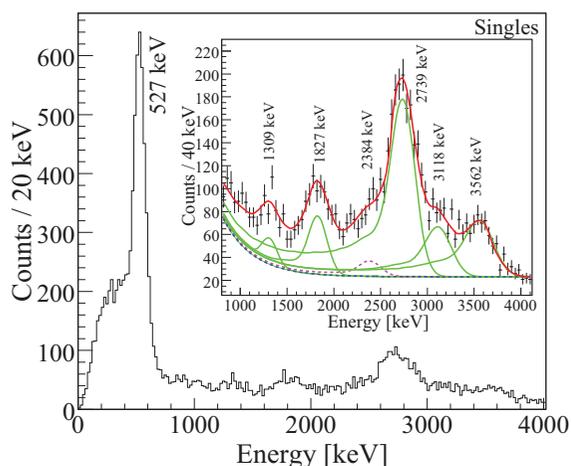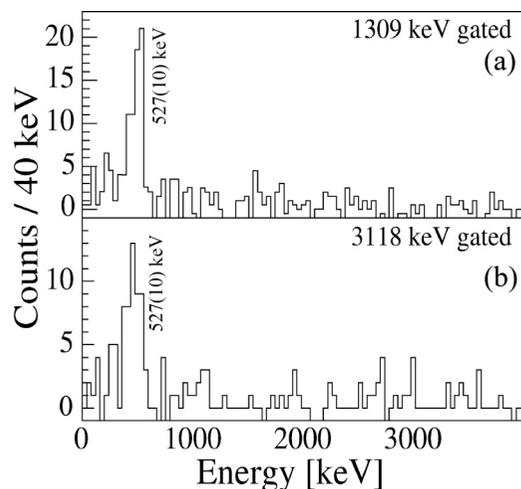


FIG. 5. $\gamma\gamma$-coincidence spectra gated by the 1309 and 3118 keV transitions measured in the in-beam data set.

simulation the energy dependence of the peak width, the cutoff energy, the Doppler shift, and the Doppler broadening were taken into account. The energy-dependent width of the $\gamma$-ray peak has been extracted from the spectroscopy of other nuclei produced in similar experimental conditions [22]. For $\gamma$ rays with energies greater than $\sim$1.5 MeV, in addition to the photo-absorption and Compton effects, pair creation also starts to play a significant role. Since an add-back procedure was used in the analysis of the $\gamma$-ray spectra, the escape of the annihilation and Compton scattered $\gamma$ rays are partially suppressed. As a consequence, the line shape is well described using a Gaussian plus a long, low-energy tail. Using the simulated line shapes the $\gamma$-ray spectrum between 2.2 and 4.0 MeV could be described by four $\gamma$ rays at 2384(64), 2739(14), 3118(33), and 3562(22) keV (inset of Fig. 4). The 2384(64) $\gamma$ line is reported as tentative.

A clear coincidence between the 527 and 3118 keV $\gamma$ rays is observed [Fig. 5(b)], establishing a state at 3639 keV excitation energy, considering that the 527 keV transition corresponds to the 521 keV $\gamma$ line observed in the $\beta$-decay experiment. No other $\gamma\gamma$ coincidences with the 527 keV line were observed, indicating that the 2384, 2739, and 3562 keV transitions decay directly to the ground state. Therefore, three new excited states are proposed at 2384(64), 2739(14), and 3562(22) keV.

## IV. DISCUSSION

The experimental level scheme deduced in the discussed experiments up to the neutron separation energy of 3.84 MeV is shown in Fig. 6. The spin and parity of the previously reported 1830 keV state [12] can be firmly established to be $1^+$ from the $\beta$ decay of $^{24}$O. The level scheme has been completed by four new states at higher excitation energy. In order to clarify their spin and parity assignment, the experimental excitation energies and branching ratios were compared to predictions of different theoretical calculations (Fig. 6). The shell-model calculations were performed using the standard USDA and USDB interactions [13,23] in the full *sd* valence space.



FIG. 4. (Color online) Singles $\gamma$-ray spectrum obtained in co-incidence with the $^{24}$F nuclei produced in the in-beam $\gamma$-ray spectroscopy experiment. The inset presents a zoom on the high-energy part of the spectrum. The lines show the result of the fit with line shapes obtained from GEANT simulation.
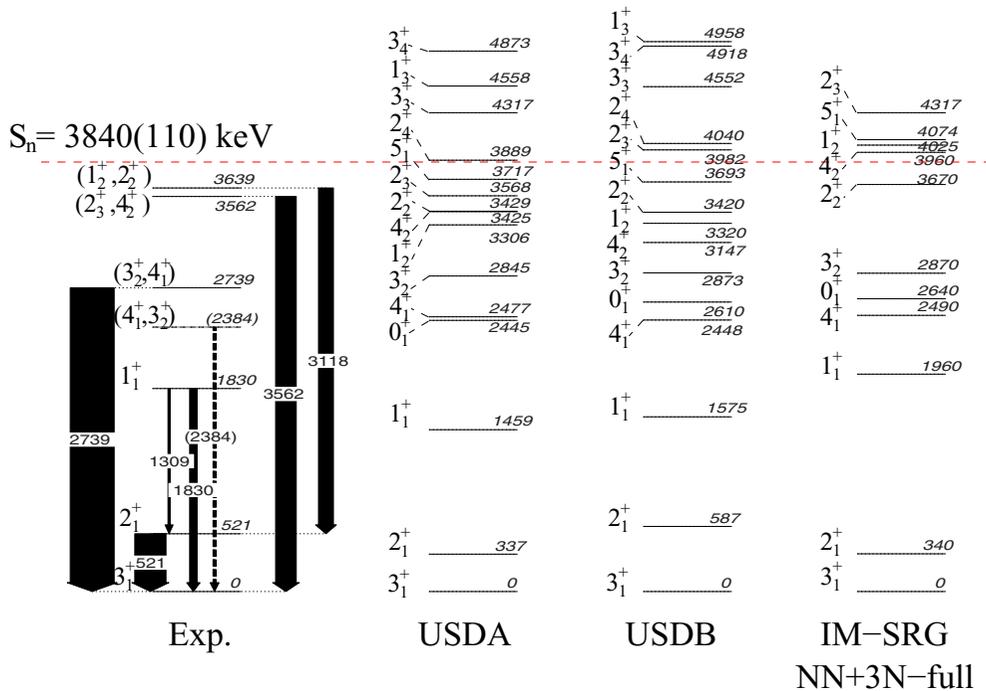
FIG. 6. (Color online) Experimental level scheme of $^{24}$F obtained in the in-beam and $\beta$-decay data set compared to shell-model calculations performed with the USDA and USDB interactions as well as *ab initio* valence-space Hamiltonians calculated from the in-medium similarity renormalization group.

To assign the spins of the observed states, the experimental branching ratios were compared to the theoretical ones extracted from the $E2$ to $M1$ decay branch of each state, rescaled in energy to match the experimental value. Starting from spin assignments of the low-energy levels, the higher-energy ones can be deduced. In the calculation of the $M1$ reduced transition probabilities, the effective $g$ factors of the proton (neutron) $g_{sp} = 5.0$ ($g_{sn} = -3.44$), $g_{lp} = 1.174$ ($g_{ln} = -0.110$), and $g_{tp} = 0.24$ ($g_{tn} = -0.16$) for the spin, orbital, and tensor components of the $M1$ operator are taken from Ref. [23]. The $E2$ reduced transition probabilities are calculated using effective charges of $1.36e$ and $0.45e$ for protons and neutrons, respectively.

The spin and parity assignment of the experimental state at 521 keV is $2_1^+$. The USDA interaction underestimates the excitation energy by $\sim 200$ keV while better agreement is found in the USDB calculations. This $2_1^+$ level decays 100% to the $3^+$ ground state of $^{24}$F. Both levels belong to the $\pi d_{5/2} \otimes \nu s_{1/2}$ multiplet with an almost pure wave function ($\sim 70\%$).

The excitation energy of the $1_1^+$ state at 1830 keV, which originates mainly ($\sim 50\%$) from a mixed $\pi s_{1/2} \otimes \nu s_{1/2}$ configuration, is underestimated in the USDA and USDB calculations. A somewhat similar shift in energy between experiment and theory is found for the $1/2^+$ state in $^{25}$F [24], which is due to an $s_{1/2}$ proton excitation. The $1_1^+$ level decays by a 1830 keV transition to the ground state [77(10)%] and by a parallel branch to the 521 keV level [23(5)%], which agrees with the USDB calculations of 72% and 28%, respectively. The USDA calculations result in 95% decay to the ground state and 5% to the $2_1^+$ level. The reduced $M1$ matrix element is 0.11 $\mu_N$ with USDA and 0.17$\mu_N$ with USDB. This difference is

consistent with the results shown in Fig. 2 of Ref. [23] where $M1$ matrix elements for USDA and USDB differ in a random way with a rms difference of about $0.10\mu_N$ being about the same for large and small values. As suggested in [23], the rms difference between experimental and theoretical $M1$ matrix elements might be reduced if some of the $M1$ data could be used to constrain the Hamiltonian.

The energy spacing of the experimental levels between 2300 and 3700 keV is better reproduced in the calculations performed with the USDA interaction. The results obtained with the USDB interaction show a spectrum with states having a regular spacing. Both calculations predict a high density of levels at high excitation energy close to the neutron separation energy.

The experimental levels at 2384 and 2739 keV decay exclusively to the ground state. The theoretical levels at approximately the same excitation energy are the $4_1^+$ and $3_2^+$ states, which have a $\sim 73\%$ and $\sim 53\%$ pure $\pi d_{5/2} \otimes \nu(d_{5/2})^{-1}(s_{1/2})^2$ configuration, respectively. The $4_1^+$ state decays directly to the ground state, on the other hand, the $3_2^+$ level has a more complicated decay pattern with parallel branches to the $3_1^+$ and $2_1^+$ states. Based on the present statistics, the spin and parity assignment of the tentative 2384 keV level and the 2739 keV state cannot be unambiguously established and both $4_1^+$ and $3_2^+$ options are left as candidates for both states.

At higher excitation energies there is a large density of calculated levels and among them the $1_2^+$ and $4_2^+$ states belonging to the $\pi d_{5/2} \otimes \nu d_{3/2}$ multiplet. These levels are of the same origin as the $1_1^+$ and $4_1^+$ states in the low-energy spectrum of the weakly bound $^{26}$F nucleus.

The experimental branching ratios were compared to the calculated decay pattern of the $4_2^+$, $2_3^+$, $2_2^+$ and $1_2^+$ levels. The $I^\pi$ of the 3562 keV level is tentatively assigned to be $4_2^+$ or $2_3^+$, and that of the 3639 keV state $2_2^+$ or $1_2^+$. The 3562 keV state is a good candidate for the $4_2^+$ which belongs to the $\pi d_{5/2} \otimes \nu d_{3/2}$ multiplet with $\sim$64% pure configuration. It would be favorably populated in the reaction due to being an yrast state. As no evidence of the existence of a $1_2^+$ state was found in the $\beta$-decay experiment, the 3639 keV state is likely to be $I = 2_2^+$. The $2_2^+$ and $2_3^+$ levels have very mixed and complex wave functions.

In addition, theoretical predictions from first-principles valence-space calculations, where the many-body processes and 3*N* forces are included are explored. Effective shell-model Hamiltonians based on *NN* and 3*N* forces were first derived for the *sd*-shell region within the context of many-body perturbation theory [3,25–28], where excitations outside the valence space were calculated to third order. There it was found that both 3*N* forces as well as an extended valence space (i.e., including orbitals beyond the standard *sd* shell), were essential to describing semi-magic isotopic and isotonic chains on top of a $^{16}$O core. The need for an extended space in the perturbative calculation of the valence-space Hamiltonian suggests that the extended orbitals need to be included nonperturbatively.

Therefore, this paper has considered a novel nonperturbative method for constructing valence-space Hamiltonians: the in-medium similarity renormalization group (IM-SRG) [14,29–31]. In addition to the IM-SRG, other *ab initio* methods have now successfully treated the oxygen chain and selected fluorines and neon isotopes with $NN + 3N$ forces [32–35]. In the IM-SRG, a continuous unitary transformation, parametrized by the flow parameter $s$, is applied to the initial normal-ordered $A$-body Hamiltonian such that undesirable off-diagonal couplings are driven to zero as $s \to \infty$:

$$H(s) = U^\dagger(s)HU(s) = H^d(s) + H^{\mathrm{od}}(s), \quad (1)$$

$$H^{\mathrm{od}}(s \to \infty) = 0. \quad (2)$$

Taking the uncorrelated ground state of doubly magic $^{16}$O, and defining $H^{\mathrm{od}}$ to be all $n$-particle–$n$-hole excitations, $H(s \to \infty)$ will flow to the fully correlated (i.e., exact) ground-state energy as $H^{\mathrm{od}}(s) \to 0$. Including excitations that connect valence-space to non-valence-space particle states in the definition of $H^{\mathrm{od}}$, the *sd* valence space will decouple from the core and higher shells as $s \to \infty$. The resulting Hamiltonian $H(\infty)$ will then consist of renormalized *sd*-shell SPEs and TBMEs, to be used as input in a standard shell-model calculation, in addition to the $^{16}$O core energy [14,30].

The starting point for these calculations are nuclear forces derived from chiral effective field theory [36,37]. We use the 500 MeV cutoff N$^3$LO *NN* potential of Ref. [38] and the local N$^2$LO 400 MeV cutoff 3*N* interaction of Ref. [39], evolved with the free-space SRG [40] to a lower momentum scale, $\lambda_{\mathrm{SRG}} = 1.88$ fm$^{-1}$. IM-SRG *sd*-shell Hamiltonians are then calculated following the procedure outlined above, based on SRG-evolved *NN* forces with 3*N* forces induced by the SRG evolution ($NN + 3N$-induced) as well as with initial 3*N* forces ($NN + 3N$-full). The latter are included through normal ordering with respect to the $^{16}$O Hartree-Fock reference state,

truncated at the two-body level [39,41]. For complete details, see Ref. [14]. Finally, the resulting shell-model Hamiltonians are diagonalized to obtain the spectrum of $^{24}$F, studying for the first time IM-SRG proton-neutron valence interactions.

Without initial 3*N* forces, the spectrum (not shown) is much too compressed and the ordering of levels is incorrect: The first eight excited states lie below 2.0 MeV, in clear contrast to experiment and the $NN + 3N$-full results shown in Fig. 6. While the ground-state energy of $^{24}$F is overbound by 7.7 MeV in the $NN + 3N$-full calculation, the predicted excited-state spectrum is in remarkably good agreement with the new experimental measurements. In particular, all excited states below the one-neutron separation threshold are less than 200 keV away from corresponding experimental levels. The only exception is a $0_1^+$ state at 2640 keV, also predicted with USDA,B, which is likely not seen experimentally due to the difficulty of the fragmentation method in populating low-*J* states. Since coupling to the continuum is currently neglected, when included, a modest lowering of the $2_2^+$, $4_2^+$, $1_1^+$, and $5_1^+$ states would be expected near threshold. Furthermore the wave functions and $\gamma$ transitions involving these states are very similar to those discussed above for USDA,B, strengthening the proposed identifications made for the $3_2^+$ and $4_1^+$ states. Specifically the $3_2^+ \to 3_1^+$ branch is 26%, in moderately better agreement with experiment. The probable identification of the 3639 keV level as the $2_2^+$ state suggests an incorrect $2_2^+$–$4_2^+$ ordering is seen in these calculations. This can be understood in terms of neglected continuum effects: The $\nu d_{3/2}$ component of the $4_2^+$ state is twice as large as that in $2_2^+$, hence one would naively expect that, when added, the continuum would then lower the $4_2^+$ by a greater amount than the $2_2^+$, possibly resulting in the correct ordering. This hypothesis needs to be confirmed by an unambiguous location of the $2_2^+$ and $4_2^+$ states in $^{24}$F and more detailed theoretical calculations. Recent coupled-cluster calculations based on optimized N$^2$LO chiral *NN* and 3*N* forces have been performed for $^{24}$F [35], which exhibit reasonable agreement with this new experimental picture.

## V. SUMMARY

Detailed spectroscopy of the $^{24}$F nucleus has been obtained at GANIL using two complementary experimental techniques: $\beta$ decay and in-beam $\gamma$-ray spectroscopy from projectile fragmentation. Previously reported transitions (521, 1309, and 1830 keV) have been confirmed, and in addition four new $\gamma$ rays have been observed for the first time. The $\gamma$-ray ordering was established from relative intensity arguments, and the large statistics of the present data allowed us to perform a $\gamma\gamma$-coincidences analysis. Gathering all the available information on $^{24}$F, a level scheme has been proposed up to the neutron separation energy. The ground state spin and parity of $^{24}$F is unambiguously determined to be $3^+$. Excitation energies and branching ratios are compared to two shell-model calculations (using the standard USDA and USDB interactions) as well as to *ab initio* shell-model calculations, using interactions derived from chiral $NN + 3N$ forces by means of the IM-SRG. From this comparison an identification of the measured states has been obtained. It is suggested that the $3_1^+$ ground state and the $2_1^+$ levels belong to the $\pi d_{5/2} \otimes \nu s_{1/2}$ multiplet

with more than 70% pure configuration. The $1_1^+$ state has a predominant $\pi s_{1/2} \otimes \nu s_{1/2}$ configuration. At higher excitation energy, the large density of observed and calculated states makes the identification of the experimental levels more ambiguous. Based on the present statistics, the spin and parity assignment of the tentative 2384 keV level and the 2739 keV state cannot be unambiguously established and both $4_1^+$ and $3_2^+$ options are left as candidates for both states. These two states have predominant $\pi d_{5/2} \otimes \nu(d_{5/2})^{-1}(s_{1/2})^2$ configurations. Tentative $2_2^+$ and $4_2^+$ spin-parity values are proposed for the 3639 and 3562 keV levels, respectively. Their ordering is only reproduced by the shell model using the USDA and USDB interactions, while the calculations performed with the IM-SRG predict an inversion of the two states. As being significantly less mixed than the $2_2^+$ state, the $4_2^+$ is expected to be more sensitive to continuum effects, and therefore the explicit treatment of such effects should lower its energy by a greater amount than the $2_2^+$. This would possibly result in the correct ordering in the IM-SRG model. Further spectroscopic information of $^{24}$F at high excitation energy and more detailed theoretical calculations will be needed to elucidate the role of the continuum in the high-energy part of the level scheme of this nucleus, but the overall agreement between IM-SRG theory and experiment is extremely satisfactory.

[1] E. Caurier, G. Martínez-Pinedo, F. Nowacki, A. Poves, and A. P. Zuker, Rev. of Mod. Phys. **77**, 427 (2005).

[2] M. Hjorth-Jensen, T. T. S. Kuo, and E. Osnes, Phys. Rep. **261**, 125 (1995).

[3] T. Otsuka T. Suzuki, J. D. Holt, A. Schwenk, and Y. Akaishi, Phys. Rev. Lett. **105**, 032501 (2010).

[4] J. D. Holt, T. Otsuka, A. Schwenk, and T. Suzuki, J. Phys. G **39**, 085111 (2012).

[5] J. Dobaczewski *et al.*, Prog. Part. Nucl. Phys. **59**, 432 (2007).

[6] M. Stanoiu *et al.*, Phys. Rev. C **78**, 034315 (2008).

[7] C. M. Campbell *et al.*, Phys. Rev. Lett. **97**, 112501 (2006).

[8] A. Lepailleur *et al.*, Phys. Rev. Lett. **110**, 082502 (2013).

[9] I. Hamamoto, Phys. Rev. C **85**, 064329 (2012).

[10] G. Hagen, M. Hjorth-Jensen, G. R. Jansen, R. Machleidt, and T. Papenbrock, Phys. Rev. Lett. **109**, 032502 (2012).

[11] A. C. Mueller *et al.*, Nucl. Phys. A **513**, 1 (1990).

[12] A. T. Reed *et al.*, Phys. Rev. C **60**, 024311 (1999).

[13] B. A. Brown and W. A. Richter, Phys. Rev. C **74**, 034315 (2006).

[14] S. K. Bogner *et al.*, Phys. Rev. Lett. **113**, 142501 (2014).

[15] R. Anne *et al.*, Nucl. Instr. Methods A **257**, 215 (1987).

[16] J. Simpson *et al.*, Acta Phys. Hung., New Series, Heavy Ion Phys. **11**, 159 (2000).

[17] V. Tripathi *et al.* (private communication).

[18] A. Lepailleur, Ph.D. thesis, Université de Caen Basse Normandie, 2014, https://tel.archives-ouvertes.fr/tel-01057890/document.

[19] E. Baron, J. Gillet, and M. Ozille, Nucl. Instr. Methods A **362**, 90 (1995).

[20] J. P. Dufour *et al.*, Nucl. Instr. Methods A **248**, 267 (1986).

[21] L. Bianchi *et al.*, Nucl. Instr. Methods A **276**, 509 (1989).

[22] M. Stanoiu, Ph.D. thesis, Université de Caen, 2002.

[23] W. A. Richter, S. Mkhize, and B. A. Brown, Phys. Rev. C **78**, 064302 (2008).

[24] Z. Vajta *et al.*, Phys. Rev. C **89**, 054323 (2014).

[25] J. D. Holt, J. Menéndez, and A. Schwenk, Eur. Phys. J. A **49**, 39 (2013).

[26] J. D. Holt, J. Menéndez, and A. Schwenk, Phys. Rev. Lett. **110**, 022502 (2013).

[27] C. Caesar *et al.* (R3B/LAND Collaboration), Phys. Rev. C **88**, 034313 (2013).

[28] A. T. Gallant *et al.*, Phys. Rev. Lett. **113**, 082501 (2014).

[29] K. Tsukiyama, S. K. Bogner, and A. Schwenk, Phys. Rev. Lett. **106**, 222502 (2011).

[30] K. Tsukiyama, S. K. Bogner, and A. Schwenk, Phys. Rev. C **85**, 061304(R) (2012).

[31] H. Hergert, S. K. Bogner, S. Binder, A. Calci, J. Langhammer, R. Roth, and A. Schwenk, Phys. Rev. C **87**, 034307 (2013).

[32] G. Hagen, M. Hjorth-Jensen, G. R. Jansen, R. Machleidt, and T. Papenbrock, Phys. Rev. Lett. **108**, 242501 (2012).

[33] H. Hergert, S. Binder, A. Calci, J. Langhammer, and R. Roth, Phys. Rev. Lett. **110**, 242501 (2013).

[34] A. Cipollone, C. Barbieri, and P. Navrátil, Phys. Rev. Lett. **111**, 062501 (2013).

[35] A. Ekström *et al.*, Phys. Rev. Lett. **113**, 262504 (2014).

[36] E. Epelbaum, H.-W. Hammer, and U.-G. Meißner, Rev. Mod. Phys. **81**, 1773 (2009).

[37] R. Machleidt and D. R. Entem, Phys. Rep. **503**, 1 (2011).

[38] D. R. Entem and R. Machleidt, Phys. Rev. C **68**, 041001 (2003).

[39] R. Roth, S. Binder, K. Vobig, A. Calci, J. Langhammer, and P. Navrátil, Phys. Rev. Lett. **109**, 052501 (2012).

[40] S. K. Bogner, R. J. Furnstahl, and R. J. Perry, Phys. Rev. C **75**, 061001(R) (2007).

[41] G. Hagen, T. Papenbrock, D. J. Dean, A. Schwenk, A. Nogga, M. Włoch, and P. Piecuch, Phys. Rev. C **76**, 034302 (2007).